Development of Chromium and Sulfur Getter for Solid Oxide Fuel Cell (SOFC) Systems

PD/PI Name, Title and Contact Information
Dr. Prabhakar Singh,
UTC Chair Professor
Materials Science and Engineering
University of Connecticut, Storrs CT
Email: prabhakar.singh@uconn.edu

Federal Agency and organization Element to which Report is Submitted
Department of Energy
National Energy Technology Laboratory

Work Performed under Federal Grant
DE-FE-0027894

Program Manager
Dr. Patcharin Burke
National Energy Technology Laboratory

Submission Date
12/16/2021

Report Submitted by
University of Connecticut, Storrs, CT 06269

Final Scientific/Technical Report

1. Programmatic Information

- **Federal Agency and organization Element to which Report is Submitted**

Department of Energy
National Energy Technology Laboratory

- **Federal Grant or Other Identifying Number Assigned by Agency**

DE-FE-0027894

- **Project Title**

Development of Chromium and Sulfur Getter for Solid Oxide Fuel Cell (SOFC) System

- **PD/PI Name, Title and Contact Information**

Dr. Prabhakar Singh,
UTC Chair Professor
Materials Science and Engineering
Email: prabhakar.singh@uconn.edu

- **Submission Date:**12/16/2021
- **DUNS Number:** 614-20-9054
- **Recipient Organization (Name and Address):** University of Connecticut, Storrs, CT 06269
- **Project/Grant Period (Start Date, End Date):** 10/01/2016-06/30/2021
- **Reporting Period End Date:** 06/30/2021
- **Report Term or Frequency Number:** F
- **Signature of the Submitting Official**

Program Manager:
Dr. Patcharin Burke
National Energy Technology Laboratory

Acknowledgment

The technical report documents and describes the work performed under Award Number DE-FE-0027894 from the US Department of Energy, National Energy Technology Laboratory.

Disclaimer

Table of Content

No.	Topic	Page No.
1.	Executive Summary	4
2.	Project objectives	4-5
3.	Summary of accomplishments	6
4.	Project Details	6-24
	Task 1: Identification of chromium and sulfur getter by 'Top-Down' approach	7-9
	Task 2: Getter development and scale up of high surface area coating with tailored porosity	9-10
	Task 3: Getter design optimization through computational analysis	10-12
	Task 4: Co-gettering testing and posttest characterization	12-23
	Task 5: Sensor development and integration in getter for in-situ monitoring	23-24
5.	Summary and conclusions	25
6.	Products	26-27
7.	References	28

2. Executive Summary

Under the "real world" SOFC operating conditions, gaseous Cr and S species coexist in air stream. The combined Cr and S effect on the electrochemical poisoning of candidate LSM and LSCF electrodes has been investigated. Electrochemical and structural analysis revealed that the combined Cr and S interactions with the LSCF electrode remains significantly different from those of the individual Cr and S interactions. S reacts with the surface SrO accompanied by morphological changes whereas the hexavalent gaseous Cr species mainly deposit at the LSCF/GDC interface as is the case with Cr-only poisoning. For LSM electrode, the combined interactions of Cr and S remains similar to the sum of individual Cr and S effects as SO_2 reacts with Sr-rich regions of the bulk LSM, while Cr deposits at the electrochemically active sites.

The use of getter, consisting of alkaline earth and transition metal oxides, has been proposed as a cost-effective approach to mitigate electrode poisoning. $SrMnO_3$ (SMO) is suggested as a robust getter material for the co-capture of airborne gaseous S and Cr species entering high-temperature electrochemical systems. The honeycomb getter forms, covered with SMO nanoparticles, were fabricated using dip coating. The SMO getter successfully maintained the electrochemical activity of LSM under the presence of gaseous Cr and S species, validating the efficacy of the getter. Post-test characterization revealed that the absorption of S and Cr contaminants led to the elongation of granular SMO particles, forming SrO nanorods and $SrCrO_4$ whiskers leaving Mn oxides underneath where inward-migrating Cr reside, indicating the high mutual affinity of Sr and Mn. The growth of reaction products during the long term exposure favors continued absorption of incoming S and Cr contaminants. The Mn_2O_9 dimers, existing on the surface, are considered to help absorb S and Cr impurities, along with the Sr-terminated surface. The SMO getter also displays robust stability in humid environments at high temperatures without phase transformation or hydrolysis, fulfilling the requirement for operation in high-temperature electrochemical systems.

3. Project objectives

The overall objective of the proposed research program is to develop and demonstrate the operation of engineered getter systems at technology readiness level (TRL)-5 for the capture of both gaseous chromium and sulfur species present in the air stream entering the solid oxide fuel cells (SOFCs) power generation systems.

The sub-objectives of the proposed program includes:

- Develop and modify chemical compositions and microstructure of getter coatings and supports using thermochemical calculation, process simulation and modeling technologies,
- Synthesize high surface area nano and meso architectures consisting of nanofiber and nanorod getter materials with micro channeled as well as porous coatings,
- Develop in-operando monitoring of the chromium and sulfur breakthrough to predict the getter health and protect the SOFC stacks,
- Scale up the getter fabrication processes
- Test validate the getter at stack and system operating conditions to demonstrate the technology readiness level at TRL 5.

The milestone log is shown in Table-1

Table 1. Milestone Log

Task/ Subtask Number	Milestone Title/Description	Start Date	Completion Date	Status	Verification Method
Subtask 1.1	Established program priorities with DOE program manager	10/1/2016	03/30/2018	Completed	Documentation
Subtask 2.1	Identified the materials chemistry	11/1/2016	12/30/2017	Completed	Thermodynamic and computational modeling
Subtask 2.2	Developed materials synthesis process for effective Cr and S getter	12/1/2016	2/28/2018	Completed	Materials characterization methods
Subtask 3.1	Optimized microstructure of the getter coatings	1/1/2017	9/30/2017	Completed	Morphological characterization
Subtask 3.2	Developed adherent porous coating on large scale substrates	3/1/2017	10/30/2017	Completed	Morphological characterization
Subtask 3.3	Surface and bulk characterization performed	4/1/2017	12/31/2017	Completed	SEM, TEM, Raman spectroscopy, FIB, FTIR
Subtask 4.1	Optimal parameters such as materials, porosity and the thickness of coating materials achieved	1/1/2017	3/31/2018	Completed	Computational analysis
Subtask 5.1	Symmetric and standard cells and getters fabricated	4/1/2017	6/30/2021	Completed	Documentation
Subtask 5.2	Getters validated in "real world" atmosphere with no degradation for 200h	5/1/2017	6/30/2021	Completed	Electrochemical impedance analysis
Subtask 5.3	Pre and post tested samples characterized	5/1/2017	6/30/2021	Completed	Materials characterization
Subtask 6.1	Developed and integrated sensor in getter bed	7/1/2017	6/30/2021	Completed	Materials and electrochemical characterization

4. Summary of accomplishments

Trace (ppm and lower) levels of airborne contaminants, present in ambient air under the real SOFC operating conditions, influence the long term electrical performance stability by adversely affecting the electrode processes and increasing the polarization losses. Combined effects of Cr and S gaseous species on the poisoning of LSM and LSCF electrodes have been studied. Chromium poisoning is mainly attributed to electrochemical reduction of Cr vapors at catalytic active sites while sulfur poisoning is primarily due to the strong chemical affinity of alkaline-earth elements with SO_2 and formation of thermodynamically stable reaction products. Experimental results indicate that the interactions of Cr/S gaseous species remain influenced by air electrode material type, operating temperature, Cr/S concentrations, and electrode polarization conditions.

The use of getters offer a cost-effective pathway for mitigating electrode contamination without the need to replace established cell and stack component materials. Considering the thermodynamics of related solid-gas reactions, the combination of alkaline-earth and transition-metal oxides Sr–Ni–O and Sr–Mn–O systems have been selected as Cr and S co-absorbent materials. Their efficacy for capturing Cr/S species was validated by electrochemical tests. Sr–Ni–O system was found to be structurally unstable accompanied by phase separation in humid environments at high temperatures (≥950 °C). Sr–Mn–O system, on the other hand, showed excellent thermal stability at higher temperature and in humid environment. Post-test characterization of the getter showed the elongation of absorbent particles and the formation of $SrSO_4$ and SrCrO4 indicating the high mutual affinity of alkaline-earth-metals and Cr/S species.

Major technical accomplishments and research findings include:

- Gas phase acidic airborne impurities react with basic air electrode constituents to form stable reaction products at the free surface and TPB.
- Thermodynamic models based on the Gibbs free energy minimization of reaction processes validate co-capture of trace sulfur and chromium impurities in a wide temperature range.
- High surface area SrNiOx (SNO) and $SrMnO_3$ (SMO) getters have been synthesized, characterized and experimentally tested.
- Supported getter structures have been fabricated using monolithic and foam substrates.
- Getter demonstrate successful capture of both Cr and S in gas phase.
- Characterization of SMO getter show high concentration of S and Cr at the inlet of the getter and negligible concentrations at the center and the outlet of the getter, indicating complete capture Posttest characterization of getters and electrochemical test sections show clean LSM/YSZ interface after 100 hrs. of electrochemical test in presence of Cr and SO2 vapor. Cr and S impurities remained present at the getter surface.

5. Project Details

The research program aims to identify candidate getter materials, fabricate getter, test and validate getter formulations to capture trace levels of intrinsic and extrinsic Cr and S gaseous species present in the air stream entering SOFC power generation systems with the objective of mitigating electrochemical poisoning of the air-electrode. Thermochemical calculations and Hydrolytic stability of the getter materials will be examined to demonstrate the structural stability of the getter under high-temperature and humid conditions representative of high-temperature electrochemical

systems operation. High surface area getter powder will be synthesized using different synthesis methods to obtain nanostructure morphology for the porous getter coating formed over ceramic substrates. Both the qualitative and quantitative characterization techniques will be used to identify surface and interfacial morphological changes and compound formation after electrochemical test. Select getter configurations will be scaled up, integrated, and tested in a prototype SOFC system test bed to validate the technology readiness level. Following sections describe the tasks and subtasks objectives along with the methodologies and approaches used for materials synthesis, experimental matrix, and characterization techniques.

5.1 Task 1: Identification of chromium and sulfur getter by 'Top-Down' approach

The objective of the proposed task is to develop cost effective getter materials for the combined capture of gaseous S and Cr species present in incoming air stream. Chemically and structurally stable SrMnO3 (SMO) getter was synthesized and honeycomb getter was fabricated by dip-coating. Stability of the getter, under SOFC operating conditions, was examined using thermochemical models.

5.1.1 Experimental methods & approaches:

The following materials were used for getter material synthesis and fabrication: strontium hydroxide octahydrate ($Sr(OH)_2 \cdot 8H_2O$; Sigma-Aldrich, USA), manganese(IV) oxide (MnO_2; Alfa Aesar, USA), strontium nitrate ($Sr(NO_3)_2$; Sigma-Aldrich), manganese carbonate ($MnCO_3$; Alfa Aesar, USA), polyvinylpyrrolidone (PVP, Sigma-Aldrich, USA), cordierite honeycomb substrate (400 cpsi; Corning Inc., USA)

The SMO honeycomb getter was fabricated by dip-coating of the cordierite ceramic backbone with an aqueous slurry. Strontium manganese oxide ($SrMnO_3$) powder was synthesized by conventional solid-state reaction of $Sr(OH)_2 \cdot 8H_2O$ and MnO_2 at 1300–1350 ˚C in ambient air followed by grinding using a planetary ball mill with alumina or zirconia milling media (Across International LLC, USA). An aqueous SMO slurry was prepared by blending as-synthesized $SrMnO_3$ powder (3.3 M) in an aqueous solution of 2.7 M $Sr(NO_3)_2$ and 3.3 M $MnCO_3$ with 33.3 g L^{-1} polyvinylpyrrolidone to improve the adhesion between the coating layer and the substrate. A cordierite honeycomb substrate with channels of 400 cells per square inch (cpsi), was submerged in the slurry followed by vacuum impregnation. The honeycomb substrate coated with the SMO slurry was dried at 60 °C for one day and then heat-treated at 1000 °C for 3 h in ambient air. X-ray diffraction (XRD) identified the as-fabricated SMO getter to be mainly composed of $SrMnO_3$.

Materials stability for the efficacy in co-capturing gas phase sulfur and chromium species was explored based on thermodynamic database (HSC database).

5.1.2 Results & Discussion:

The compounds probable to form by the reaction between alkaline earth metals (Mg, Ca, Sr, and Ba) and Cr and S species are listed in Table 2. To estimate the absorption capability of the alkaline earth metals, the equilibrium partial pressures of $CrO_2(OH)_2$ (g) and SO_2 (g) evolved from the resulting Cr and S compounds were calculated using HSC Chemistry 6.0 (Outotec, Finland).

Table 2. Melting and eutectic points of possible compounds in M–Cr–O and M–S–O systems (where, M = Mg, Ca, Sr, and Ba) [1–3].

Elements	**M–Cr–O compounds (Tm)**	**M–S–O compounds (Tm)**
Mg[a]	$MgCr_2O_4$ (2350 °C)	$MgSO_4$ (1124 °C)
Ca	$xCaO•yCrO_3•zCr_2O_3$ + $CaCrO_4$ (1022 °C)	$CaSO_4$ (1460 °C)
Sr	$SrCrO_4$ (1253 °C)	SO_2 (1606 °C)
Ba[b]	$BaCrO_4$ (major) + $Ba_3Cr_2O_6$ + $BaCr_2O_4$ (1250 °C)	$BaSO_4$ (1580 °C)

a. Mg is explosive upon heating in air.
b. Ba is likely to exist as $BaCO_3$ because of its high affinity to CO_2.

The stability of host materials and reaction products under system operating conditions were considered. Mn and Fe among transition metals were chosen as they are non-noble metals (cost-effective) with multiple chemical states. The stability of Sr–Mn–O and Sr–Fe–O systems at elevated temperatures and in humid atmospheres, were assessed based on the phase diagrams and the analysis of structural changes. Sr–Fe–O system showed phase change at ≥ 775 °C, whereas the Sr–Mn–O system showed the bulk phase stability up to 1215 °C. Initial laboratory tests also showed that while SrFeO3 is readily pulverized by reacting with moisture ($SrFeO_3$ + H_2O → $SrFe_{12}O_{19}$ + $Sr_3Fe_2(OH)_{12}$ + $Sr(OH)_2•8H_2O$), $SrMnO_3$ remains stable during such exposure. Strontium manganese oxide was therefore selected for further study.
Surface morphological analysis by scanning electron microscopy (SEM) show that the honeycomb getter is uniformly coated with granular SMO particles with a thickness of ~5 μm (Figure 1). The honeycomb architecture is intended to permit steady, incompressible, and laminar flow of the airstream for SOFC systems, and the structural design can be modified depending on the system size and operating conditions, as shown by earlier simulation work [4].

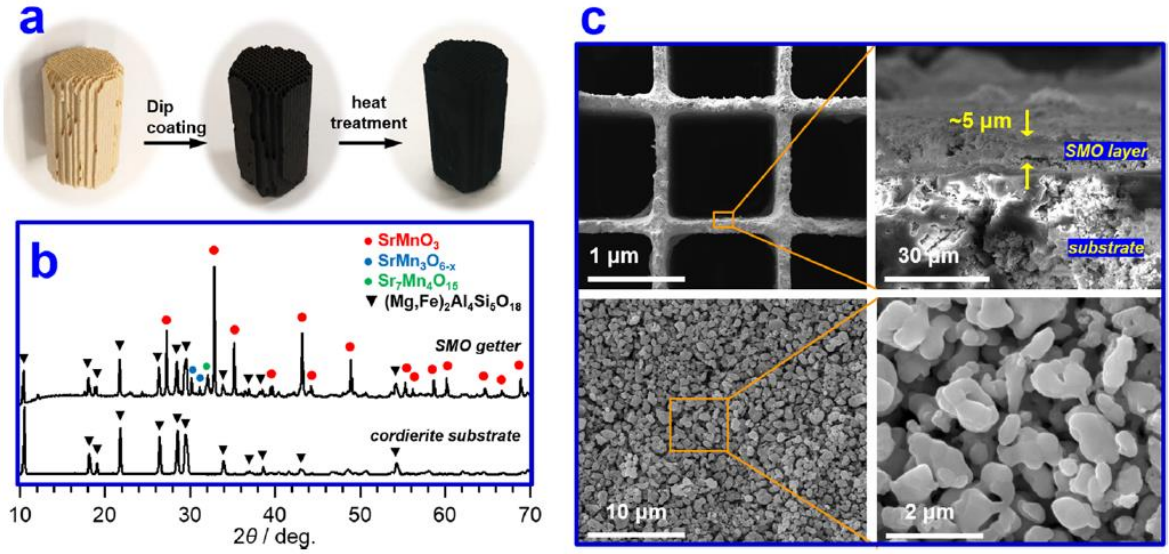

Figure 1. (a) Fabrication of the SMO getter by dip-coating of a cordierite honeycomb substrate (400 cpsi) in an aqueous precursor slurry, followed by heat treatment (b) XRD patterns of a bare cordierite substrate and the SMO getter (indexed on the basis of JCPDS data), (c) SEM images of the cross section and surface of the SMO coating layer on the substrate.

5.2 Task 2: Getter development and scale up of high surface area coating with tailored porosity

A number of novel approaches consisting of conductive coatings on the metallic interconnect to prevent direct exposure to cathode atmosphere, modified cathode chemistry as well use of alloy chemistry that forms non-chromia scales have been proposed to mitigate the cathode poisoning and electrical performance degradation. The above approaches, however, have limitations which do not prevent the long-term chemical and structural deterioration resulting in electrochemical performance degradation. Co-capture of chromium and sulfur before these species poison the cathode is the key to mitigate the performance degradation and extend the SOFC stack lifetime. We considered the use of high surface area Sr base compounds as low-cost materials with excellent tendency to capture Cr and S.

High surface area (HSA) nanofibers and nanorods based getter materials with nano and meso architectures have been synthesized and characterized by XRD, SEM, and TEM techniques. Several experimental methods have been utilized for the synthesis of high surface area (HSA) nanofiber material for enhanced getter capture efficiency. Three getter types, consisting of manganese oxide octahedral molecular sieves (OMS-2), cordierite honeycomb, and Al_2O_3 micro fiber substrates, have been used to support nanostructured getter materials. Hydrothermal method was used to synthesize high surface area SrO-MnO which works as active getter material on cordierite or Al_2O_3 microfiber. An optimized synthesis protocol to synthesize high surface are getter material have been proposed and validated.

5.2.1 Experimental methods & approaches:

High surface area SMO/SNO powder was synthesized using co-precipitation method. In a 2000 ml beaker, 200 ml of de-ionized water was mixed with 148.45g of Sr(NO3)2, and 176.07g of Mn(NO3)2. 4H2O for 100 g high surface area (HSA) SMO powder synthesis. For 100 g HSA SNO powder synthesis, 200 ml of de-ionized water was mixed with 144.64g of Sr(NO3)2, and 198.75g of Ni(NO3)2*6H2O. Solutions were stirred and heated on a hotplate set to 80 C. Subsequently, the pH of the solution was raised to 8.5 by adding stock 27-30%mol NH_4OH dropwise. The extra water was evaporated from solution by drying overnight on hotplate or dry oven to achieve a wax/gel. The formed metal was separated from residual ammonium nitrates via centrifugation. The final powder was dried in an oven at 120 C overnight to collect high surface area precursor powder for SMO/SNO getter [5].

The strontium manganese oxide getter was fabricated by dip-coating of cordierite honeycomb substrates. The fabricated getter was used for the electrochemical evaluation of the electrode and co-capture of Cr and S contaminants. The morphological, elemental and particle sizes of the high surface area analyses were performed using a FEI Quanta 250 FEG scanning electron microscope attached with an energy dispersive X-ray spectroscope (EDS). Getter chemistry and phases were analyzed using Bruker AXS D-8 Advance X-ray diffractometer (XRD)

5.2.2 Results & Discussion:

Figure 2 shows the morphologies of the high surface MnO_2 nanofiber on the cordierite support. Other active components such as SrO and NiO are coated on these MnO_2 nanofibers by

impregnation technique. Due to the small diameter of the MnO_2 nanofibers, the coating layer has a high surface area (30-65 m^2/g) for sulfur and chromium co-capture.

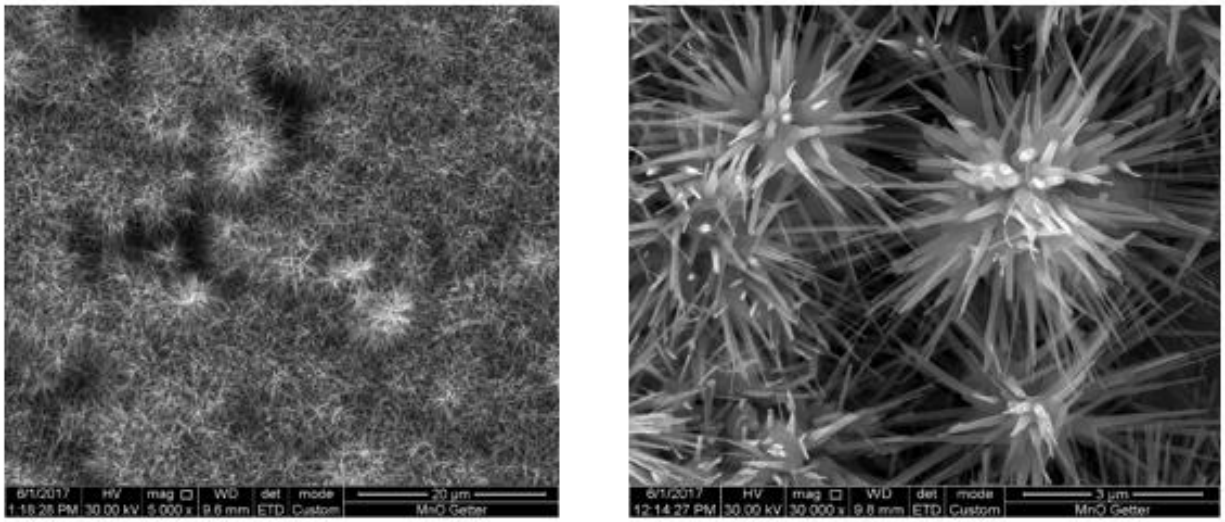

Figure 2. SEM images of HSA SrO-MnO nanofibers coatings on the cordierite support

To develop getter using HSA SMO/SNO, the pre-fired cordierite support, free of organics, was used to achieve a uniform coating layer (~2-10 µm) of SMO/SNO on the cordierite support as shown in the Figure 3. Subsequently, the coating materials along the support was calcined at high temperatures (710 to 900 °C) for 2-10 hrs. Uniformly coated cordierite getters were evaluated for contaminant capture by electrochemical tests.

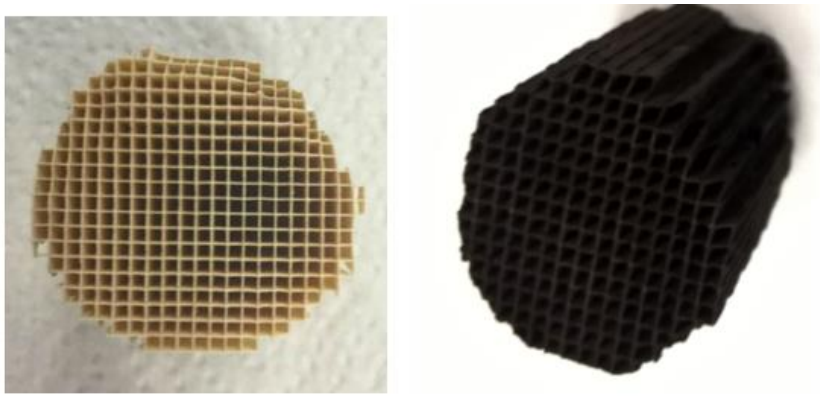

Figure 3. One-inch diameter cordierite support and a cordierite supported MnO-SrO getter

5.3 Task 3: Getter design optimization through computational analysis

Materials chemistry and formulations for the co-capture of gas phase sulfur and chromium species was explored based on thermodynamic and computational materials modeling and design to develop suitable oxides and related compounds with ability to simultaneously capture sulfur and chromium species present in hot air (contacting chromia forming alloys) entering the SOFC stack. Co-stability of reaction products formed under SOFC operating conditions was established under a range of temperature and contaminant concentration conditions.

5.3.1 Experimental methods & approaches:

Thermochemical data, utilized for the development of reaction models, were obtained from the Thermochemistry software HSC chemistry. The software allows the analysis under a wide range of temperature and pressure. The thermochemical data also help in comparing the stability of candidate getter materials under SOFC operating conditions of interest.

5.3.2 Results & Discussion:

The phase stability of SrO was analyzed under different partial pressure of Cr and S gas species. Figure 4 shows the phase diagram of SrO in the presence of $CrO_2(OH)_2$(g) and SO_2 (g) at 750 °C. Under these atmospheric conditions, both $SrSO_4$ and Cr_2O_3 are expected to be produced under the SOFC cathodic condition (as marked by a red spot in Figure 4).

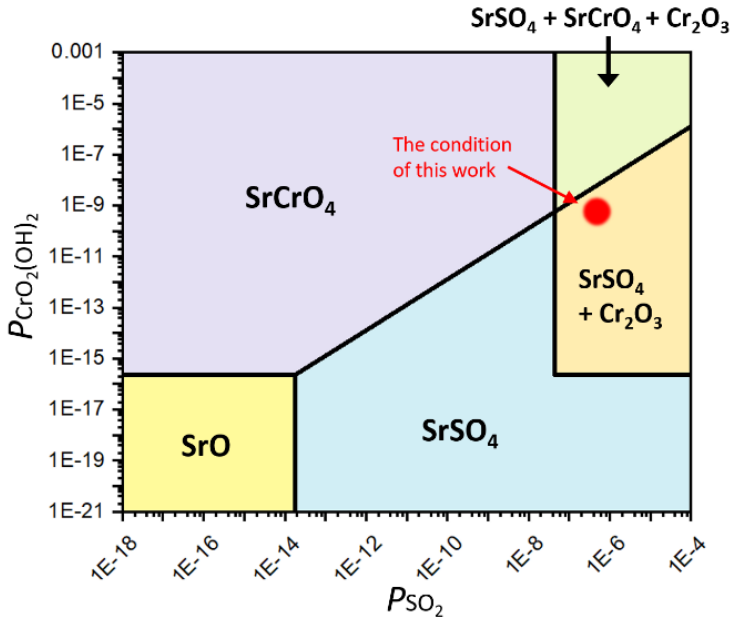

Figure 4. Phase stability diagram for a fixed SrO and varying partial pressures of SO_2 and $CrO_2(OH)_2$ at 750 °C. The red spot indicates the partial pressures of the chromium and sulfur species in this work.

Alkaline earth elements have been considered as the materials of choice for the capture of gaseous Cr and S species before cathodic interaction, because of their affinity to form stable Cr and S containing compounds as demonstrated by large free energy minimization of the reactions. It is recognized that alkaline oxides have high reactivity with SO_2 (high to low: Sr > Ca > Ba > Mg) for the formation of respective sulfates. For instance, SrO and BaO, segregated onto the surface of SOFC cathodes readily react with airborne Cr and S species. CaO is also capable of scavenging Cr vapors as well as SO_2 evolved during coal combustion. Relative stability of reaction products and the reactivity of the alkaline earth metals with trace gaseous Cr and S contaminants were examined using the equilibrium partial pressures of $CrO_2(OH)_2$ (g) and SO_2 (g) calculated using HSC Chemistry 6.0 (Outotec, Finland) as shown in Figure 5.

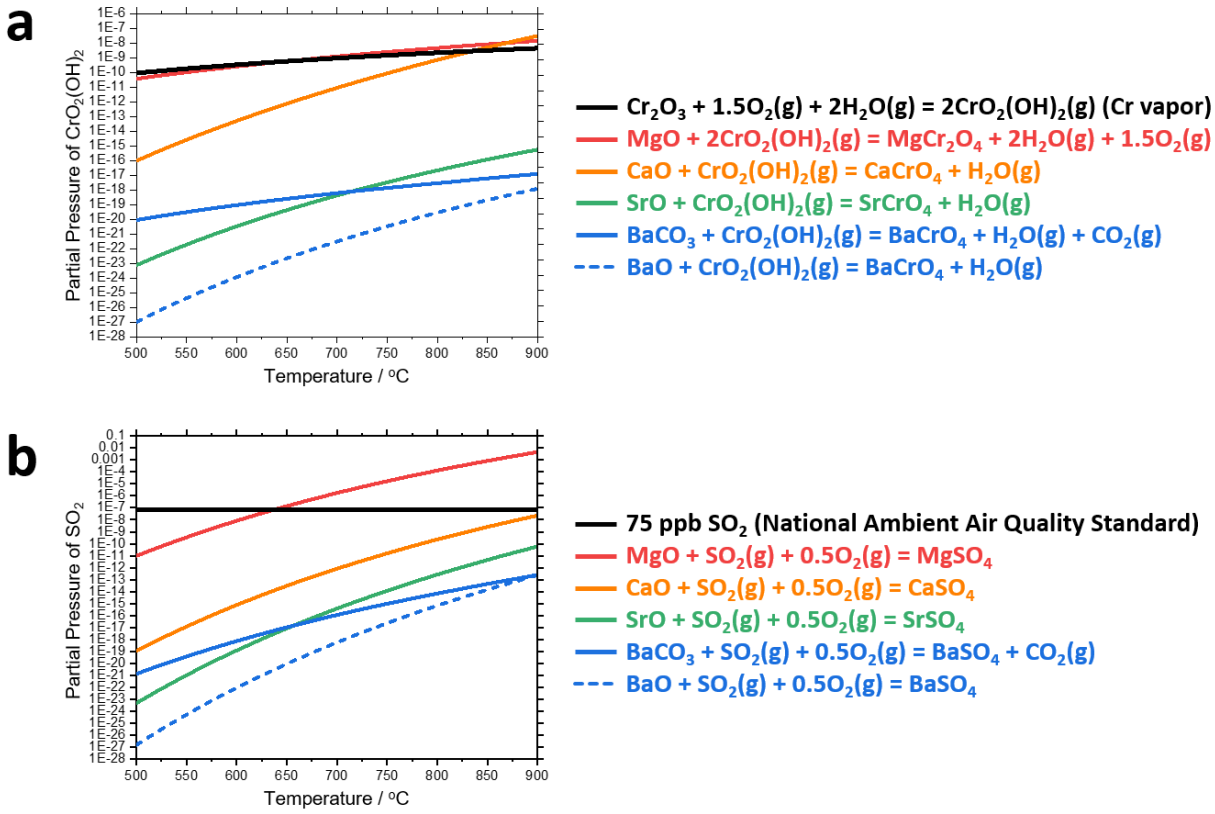

Figure 5. Partial pressures of (a) $CrO_2(OH)_2$ (g) and (b) SO_2 (g) from the composites of alkaline earth metals (Mg, Ca, Sr, and Ba) and chromium/sulfur: $MgCr_2O_4$, $CaCrO_4$, $SrCrO_4$, $BaCrO_4$, $MgSO_4$, $CaSO_4$, SO_2, and $BaSO_4$ (HSC database).

5.4 Task 4: Co-getter testing and posttest characterization

High surface area getter was used for the co-capture of Cr and S to mitigate degradation of electrochemical performance of SOFC. The SMO getter with a 3D honeycomb architecture successfully maintains the electrochemical activity. Unlike the previously developed SNO getter, the SMO getter displays robust stability at high temperatures and in humid environments without phase transformation and hydrolysis.

5.4.1 Experimental methods & approaches:

For electrochemical characterization, half cells were fabricated and electrically tested under desired temperature and gas flow conditions. LSCF- and LSM-based electrodes were tested for the evaluation of poisoning mechanism. 25 mm diameter electrochemical cells containing Gd-doped ceria (GDC; $Gd_{0.10}Ce_{0.90}O_{1.95}$; Fuelcellmaterials, USA) and yttria-stabilized zirconia (YSZ; 8 mol.% yttria; Fuelcellmaterials, USA) were fabricated. The $(La_{0.60}Sr_{0.40})_{0.95}Co_{0.20}Fe_{0.80}O_{3-\delta}$ and $(La_{0.80}Sr_{0.20})_{0.95}MnO_{3\pm\delta}$ slurries (Fuelcellmaterials, USA) were thoroughly mixed with an ink vehicle (terpineol-based; Fuelcellmaterials, USA) and then screen-printed onto the GDC and YSZ electrolyte supports, respectively, using a screen printer (Model 810, Systematic Automation Inc., USA). Cells were subsequently sintered in air at 1200 °C for 2 h with a ramp rate of 3 °C min^{-1}. Each electrode surface was connected with Pt current collector using Pt gauze and paste. In the

same manner, the opposite side of the electrode was attached with Pt gauze and wire. The edge of the electrolyte was also connected to a Pt wire as a reference electrode. The assembled cells (LSCF|GDC|Pt and LSM|YSZ|Pt) were heated at 850 °C for 1 h in air for complete adhesion of the Pt paste. The as-prepared cells were sealed onto an alumina tube using an alumina paste,. The Pt wires, connected to the electrodes and electrolytes, were linked to a potentiostat (VMP3, Bio-Logic, France).

The electrochemical tests were carried out at 750 °C under the flow of air containing both SO_2 gas (500 ppb) and Cr vapors (~1 ppb $CrO_2(OH)_2$ gas), where the concentration of SO_2 gas was precisely controlled by a gas mixing system (Series 4000, Environics, USA) while the Cr vapors were generated from Cr_2O_3 pieces wrapped with silver gauze under humidified air flow(~1.5% H_2O) (Figure 6). Electrochemical impedance spectroscopy (EIS) for the as-prepared LSCF|GDC|Pt and LSM|YSZ|Pt cells was conducted for 110 h under a bias of 0.5 V in the frequency range from 0.5 Hz to 200 kHz with a 10 mV sinus amplitude at an interval of 1 h.

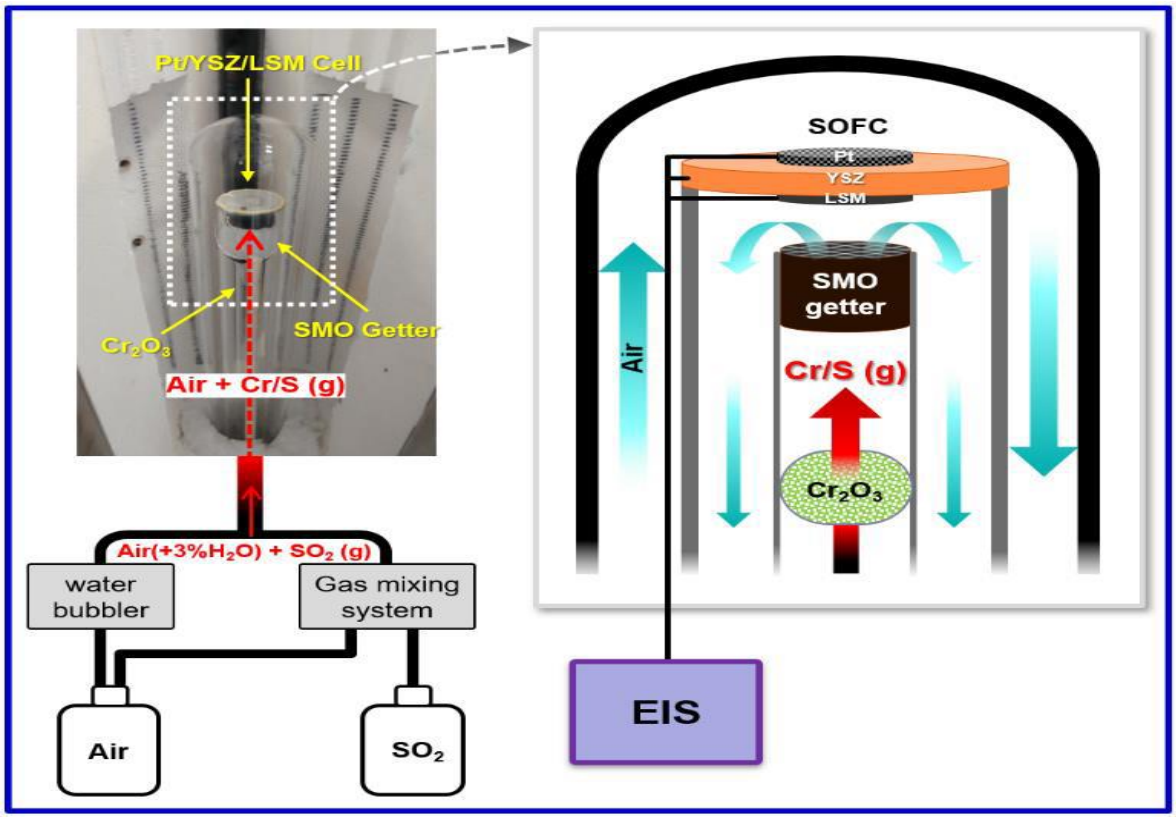

Figure 6. Schematic of the test setup utilized for EIS measurement on the LSM|YSZ|Pt cell in the presence of Cr vapor and SO_2 gas through the SMO honeycomb getter.

<u>In Operando Electrochemical Tests with SMO getter:</u> The capture of gaseous S and Cr species over the SMO getter was investigated using electrochemical impedance spectroscopy (EIS) technique. The EIS tests were conducted at 650–700 ˚C under the three different conditions as follows: (a) the flow of air-SO_2 without the getter, (b) the flow of air-Cr vapor without the getter, and (c) the flow of both air-Cr vapors and air-SO_2 with the getter. The spectra were recorded under

a bias of 0.5 V in the frequency range from 0.5 Hz to 200 kHz using a sinus amplitude of 10 mV at an interval of 1 h. During the test (a), 4 ppm SO_2 gas, mixed with humidified air (~3% H_2O by water-bubbling), was injected into the LSM cathode chamber (120 SCCM) for 100 h (110–210 h) after the electrode activation for initial 110 h under the flow of humidified air. During the measurement for the test (b), air- Cr vapor (i.e., ~1 ppb $CrO_2(OH)_2$ (g)) flowed (120 SCCM) over the LSM cathode for 100 h. Humid air flowed through the Cr_2O_3 pieces to generate the Cr vapor. For the Test (c), the SMO honeycomb getter was inserted in the alumina tube one inch away from the cathode.

Evaluation of the hydrolytic and thermal stability**:** To examine the getter material stability against hydration and exposure to humidity, a SMO pellet (φ = 13 mm) was placed in a humid environment (2.7% H_2O, measured by a ThermoPro hygrometer), and the shape and color were visually observed for 12 days. The $SrMnO_3$ powder, also exposed to the humid environment for 14 days and soaked with distilled (DI) water for one day, was analyzed using XRD technique. The thermal stability of $SrMnO_3$ was also evaluated employing in situ high temperature (HT) XRD. During the HT-XRD analysis, the SMO powder was heated up to 900 °C at a ramp rate of 5 °C min^{-1}. The XRD patterns were recorded at ~25, 500, 700, 900 °C, and room temperature (after cooling down).

In addition, the XPS depth profiling was carried out using a Quantum 2000 scanning ESCA microprobe (Physical Electronics, USA) on the SMO pellet obtained by heat-treatment at 700 °C for 100 h and immediate cool-down at 10 °C min^{-1}. The morphology and elemental composition of the electrodes were analyzed by scanning electron microscopy (SEM; Quanta 250 FEG, FEI, USA) equipped with energy-dispersive X-ray spectroscopy (EDS). The electrode/electrolyte cross-sectional analysis was performed using a focused ion beam (FIB, FEI Strata 400s Dual Beam FIB, USA). The nanostructure and elemental distribution were obtained by scanning transmission electron microscopy (STEM; Talos F200X S/TEM; FEI, USA) at 200 kV. The reactions between surface-SrO and Cr/S contaminants were thermodynamically calculated from the database in HSC Chemistry (Outotec, Finland).

5.4.2 Results & discussion

Figure 7a shows the degradation in electrochemical performance of LSM|YSZ|Pt and LSCF|GDC|Pt cells under the flow of humid air-SO_2 (g) and humid air-Cr vapors. The current density of the LSM-based cell rapidly decreased for the first ~10 h, while that of the LSCF-based cell reduced gradually. Nyquist plots (Figure 7b & 7c) show that the polarization resistance increases in both cell whereas ohmic resistance changes in only LSCF-based cell.

Figures 8a and 8b show the cross-sectional SEM images of LSM before and after the exposure to Cr vapor and SO_2 containing air under experimental conditions. The granular morphology of LSM with a smooth surface did not change after the exposure to Cr and S contaminants (Figure 9). Elemental distributions of Cr and S are very similar to those in the LSM poisoned by Cr only and S only contaminants [4,6–8]. Figures 10c and 10d show the morphology of LSCF before and after the exposure to gaseous Cr and S contaminants under polarization conditions. Initially smooth morphology changed to an angulated over the exposed areas indicating that the morphology change of the LSCF particles is mainly due to contaminant incorporation.

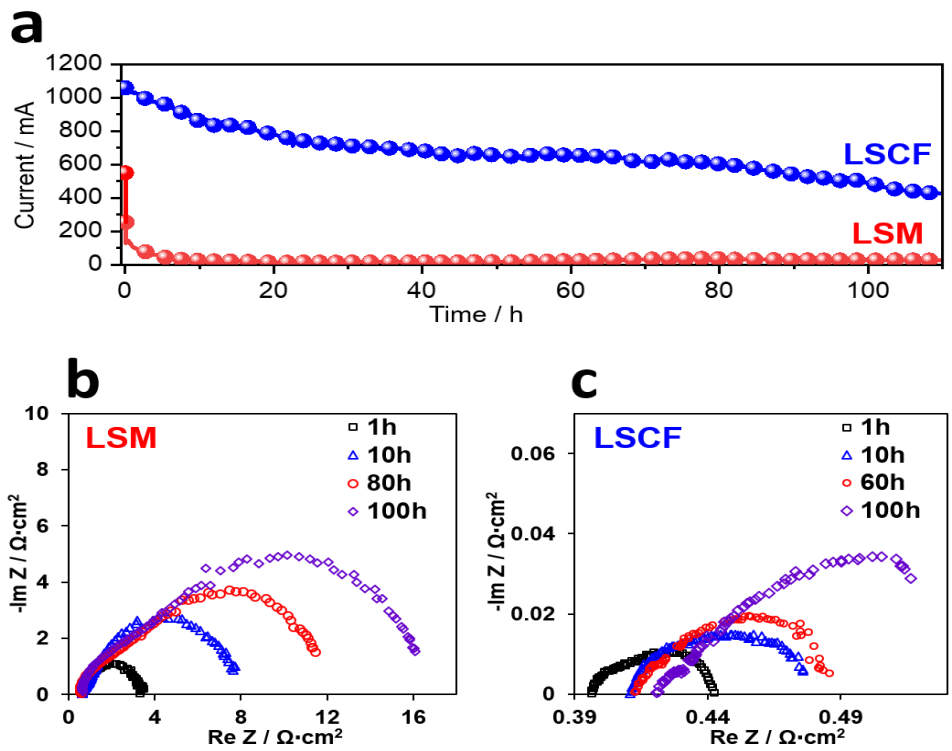

Figure 7. (a) Current densities and (b and c) Impedance spectra of LSM|YSZ|Pt and LSCF|GDC|Pt solid oxide cells recorded over time (up to 110 h) at 750 °C under the flow of 500 ppb SO_2 (g) and Cr vapor (~1 ppb $CrO_2(OH)_2$ (g)) toward the LSM and LSCF air-electrodes.

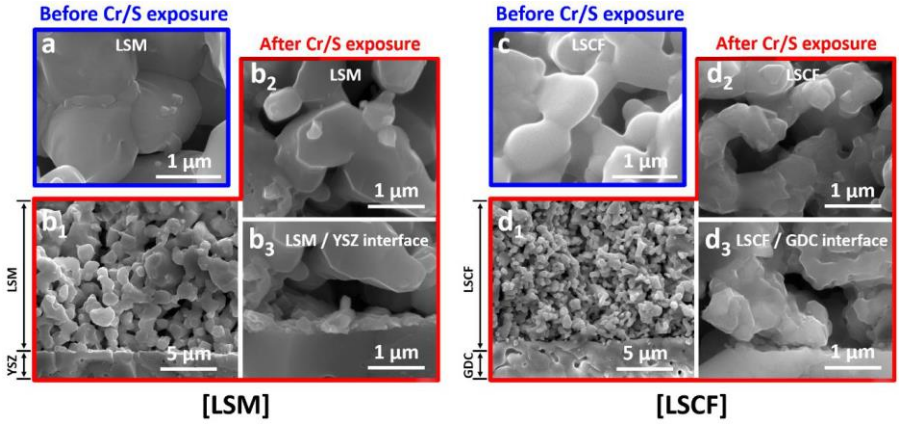

Figure 8. Cross-sectional SEM images of pristine LSM and LSCF electrodes (a and c) and those exposed to SO_2 gas and Cr vapors for 110 h at 750 °C during the electrochemical test (b and d).

Combined Cr and S Poisoning processes in LSM: Figure 9a shows STEM elemental images of the LSM electrode after the exposure to gaseous Cr and S contaminants. Cr rich deposits are located at the TPB phase near the LSM/YSZ interface, as occurring via the following electrochemical reduction reaction from Cr^{+6} to Cr^{+3} [4]:

$$2CrO_2(OH)_2\ (g) + 3V_{O}^{\bullet\bullet} + 6e^- = Cr_2O_3\ (s) + 2H_2O + 3O_O^X$$

In addition, sulfur rich particles are identified in the Sr-rich areas of the tested LSM electrode which may indicate absorption and interaction of SO_2 (g) onto Sr-terminated LSM surface with

the formation of SO_2 (Figure 9a). Further analysis using high-resolution (HR) TEM and Fast-Fourier transform (FFT) technique confirms SO_2 (orthorhombic, Pbnm, a = 6.87 Å, b = 8.37 Å, and c = 5.36 Å) as a secondary phase of LSM under SO_2. A similar analysis was carried out on the Cr-rich area (Figure 9b) at the TPB region and observed formation of SrCrO4. This is in good agreement with the prediction that the Cr deposition was attributed more to electrochemical reduction reaction than to chemical reaction.

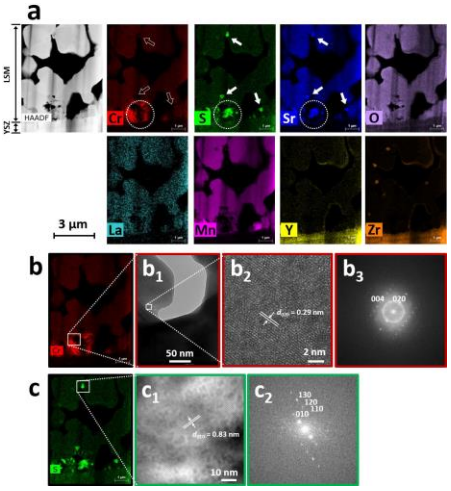

Figure 9. (a) STEM High-angle annular dark-field (HAADF) and elemental mapping images (Cr, S, Sr, O, La, Mn, Y, and Zr) of the cross section of the LSM/YSZ interface exposed to SO_2 gas and Cr vapors at 750 °C for 110 h during the EIS test. (b) High-resolution TEM images and Fast Fourier Transform (FFT) patterns of the Cr-rich region and (c) the S-rich region.

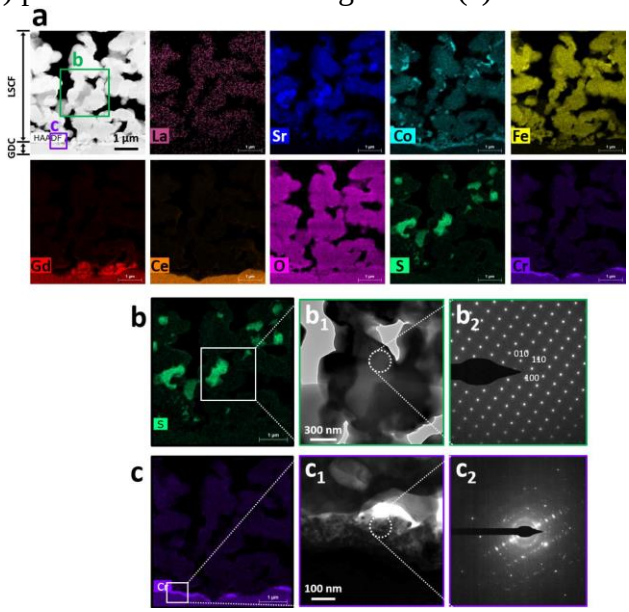

Figure 10. (a) STEM High-angle annular dark-field (HAADF) and elemental mapping images (La, Sr, Co, Fe, Gd, Ce, O, S, and Cr) of the cross section of the LSCF/GDC interface exposed to SO_2 gas and Cr vapors at 750 °C for 110 h during the EIS test. (b) High-resolution TEM images and selected area electron diffraction (SAED) patterns of the grains at the LSCF and (c) at the LSCF/GDC interface.

Combined Cr and S poisoning processes in LSCF: Figure 10a shows STEM elemental images of the cross section of LSCF electrode after the electrochemical test in the presence of Cr and S contaminants. Interestingly, it is observed that Cr resides predominantly at the LSCF/GDC interface (Figure10: Cr). This tendency is different from that of Cr-only poisoning in LSCF, where Cr is mainly deposited on the LSCF surface by reacting with surface-segregated SrO to form $SrCrO_4$ [8–10]. The deposition of Cr at the interface is attributed to the electrochemical reduction reaction, similar to the case of Cr poisoning in LSM. Sulfur, on the other hand, is distributed in Sr-enriched regions of LSCF (Figure 10: S, and Sr), implying the reaction of segregated SrO with SO_2 (g). This result somewhat deviates from the case of S-only poisoning of LSCF, where sulfur is concentrated near the LSCF/GDC interface owing to the high concentration of oxygen vacancies [11,12]. Figure 10b shows the HR-TEM image of an S-rich area of LSCF particles and the corresponding SAED pattern. The pattern is identified as SO_2 (orthorhombic, Pbnm, a = 6.87 Å, b = 8.37 Å, and c = 5.36 Å), confirming the chemical reaction of Sr with SO_2. Figure 10c shows the HR-TEM image and SAED pattern of Cr-rich nanoparticles at the LSCF/GDC interface. The structure of the nanosized Cr compound could not be exactly determined by the SAED pattern with halo rings but is regarded as Cr_2O_3 by thermodynamic considerations, based on previous studies [13,14] . It is considered that the surface segregated SrO in LSCF loses the ability to capture Cr vapors due to adsorption/absorption of SO_2, thereby allowing Cr vapors to pass through LSCF and reach the electrode/electrolyte interface.

For LSM, the combined Cr/S poisoning behavior is equivalent to the sum of those of individual Cr and S poisonings. In LSCF, Cr_2O_3 is deposited at the LSCF/GDC interface and SO_2 on the LSCF particle surface (combined Cr/S poisoning). From the thermodynamics of the SrO–$CrO_2(OH)_2$–SO_2 system (Figure 4), it is found that the reactions between surface-segregated SrO and Cr/S contaminants prefer to form $SrSO_4$ rather than $SrCrO_4$ under the experimental condition. At high temperatures (> 500 °C), Sr-segregation occurs to form SrO on LSCF surfaces, which is highly reactive with Cr/S contaminants[15]. The surface SrO is more likely to react with SO_2 than Cr vapors by physical/chemical absorption. Continuous absorption and reaction lead to the formation of $SrSO_4$ on the LSCF particle surface. In the case of Cr vapors flowing over LSCF, since the surface Sr is covered by physi/chemisorbed SO_2, the SrO's ability to capture Cr species is diminished. Thus, the Cr vapors freely reach the LSCF/GDC interface resulting in the deposition of Cr oxides by electrochemical reduction reaction.

The absorption capability of SMO getter for airborne Cr and S contaminants was evaluated using solid oxide cells (LSM|YSZ|Pt) under the flow of humidified air containing 4 ppm SO_2 and ~1 ppb $CrO_2(OH)_2$ (evolved from Cr_2O_3) toward the LSM cathode through the SMO getter. This performance was compared with those recorded under the flow of either the SO_2 or $CrO_2(OH)_2$ gases in the absence of the getter. The current density remained stable under the flow of humidified air (~3% H_2O by water-bubbling) (Curve (a) in Figure 11:0–110 h). Immediately after the injection of 4 ppm SO_2 gas, the current density gradually decreased (Curve (a) in Figure 11: 110–150 h). Similarly, under the generation of Cr vapor, the current density rapidly dropped (Curve (b) in Figure 11). The electrode performance degradation by Cr-poisoning is due to preferential Cr deposition at the triple phase boundary (TPB) via the following electrochemical reduction.

$$2CrO_2(OH)_2\ (g) + 6e^- \rightarrow Cr_2O_3 + 2H_2O + 3O^{2-}$$

In contrast, the degradation by S-poisoning is due to the chemisorption of SO_2 on the LSM surface, resulting in SO_2 precipitation and non-stoichiometric, Sr-depleted LSM. In the presence of SMO getter, the current density remained stable for 230 h (Curve (c) in Figure 11) despite the injection of the same levels of Cr vapor and SO_2 gas (i.e., ~1 ppb $CrO_2(OH)_2$ for the initial 100 h, and then both ~1 ppb $CrO_2(OH)_2$ and 4 ppm SO_2 for another 120 h). cross-section of the LSM tested in the presence of the SMO getter under the flow of Cr and S gases shows a clean surface morphology whereas the sulfur-contaminated LSM shows a modified surface with nano protrusions of SO_2 precipitates.

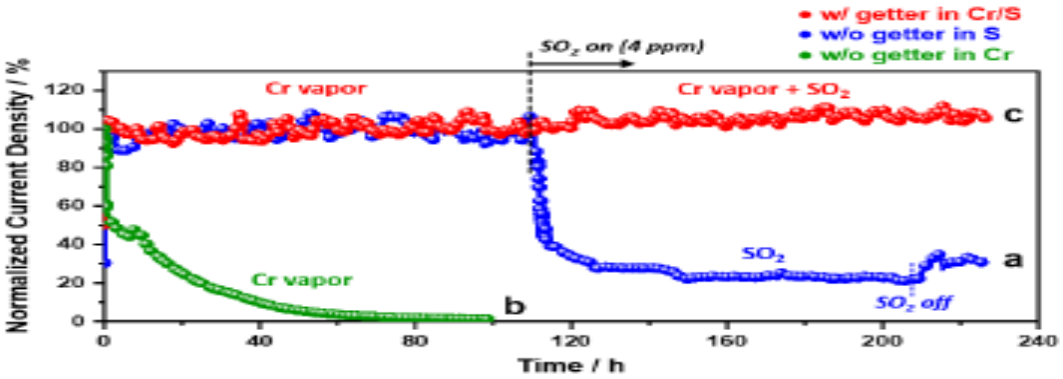

Figure 11. Current density of the LSM|YSZ|Pt cells over time under the flow of either (a) 4 ppm SO_2 gas (injected after 110 h) or (b) Cr vapor (~1 ppb $CrO_2(OH)_2$) toward the LSM cathode in the absence of SMO getter, and (c) that recorded under the flow of both Cr vapor and 4 ppm SO_2 gas (injected after 110 h) toward the LSM cathode through the SMO getter.

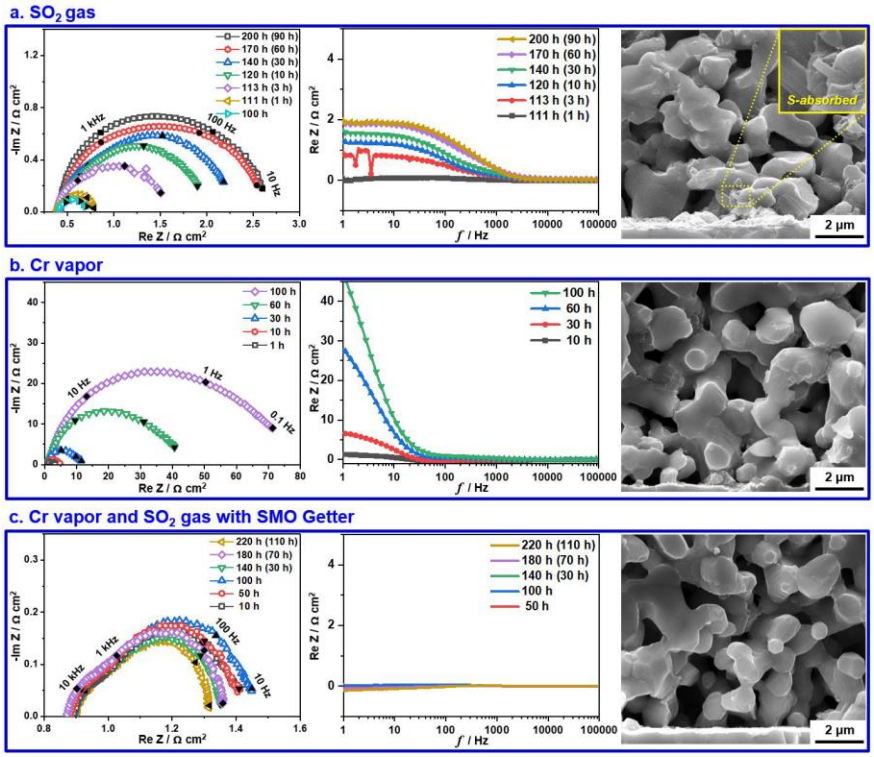

Figure 12. Impedance spectra (Nyquist and Bode plots) of the LSM|YSZ|Pt cell and cross-sectional SEM images at the LSM/YSZ interface exposed to (a) SO_2 gas, (b) Cr vapor, and (c) both Cr vapor and SO_2 gas in the presence of the SMO getter, respectively.

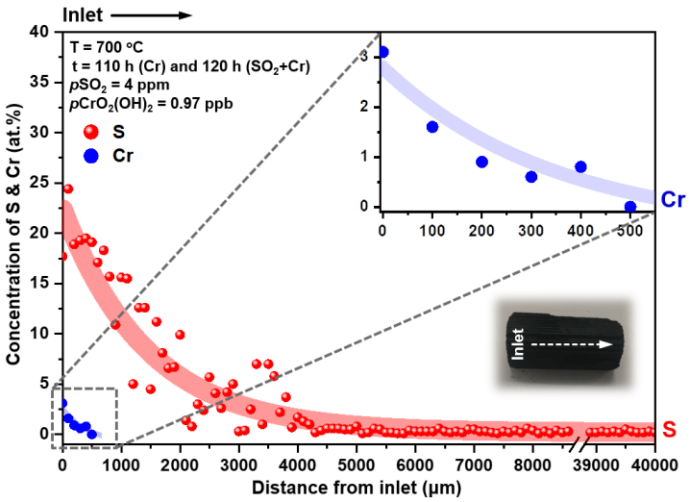

Figure 13. Distribution of S and Cr along the inner channel from the inlet to the outlet of the SMO getter that was exposed to 4 ppm SO_2 (120 h) and ~1 ppb Cr vapor (230 h) at 700 °C during the EIS test, analyzed using EDS.

Figure 13 shows the concentration of Cr and S along the air flow path in the inner channel of the posttest SMO getter which reveals that highest concentration of S and Cr to be at the getter inlet. The concentration then decreases along the air flow path in the getter channel towards the outlet, indicating SMO's ability to capture both S and Cr gaseous species in air. In addition, the morphological observation (Figure 14) shows the transformation of the microstructure along the channel length from oblong (0–2 mm) and angular (2–4 mm) to spherical (at a distance of > 4 mm) shapes. Figure 14a shows the surface morphology along the channel length. It appears that the morphology transformed from spherical to angular to whisker-like shapes as the Cr concentration increases.

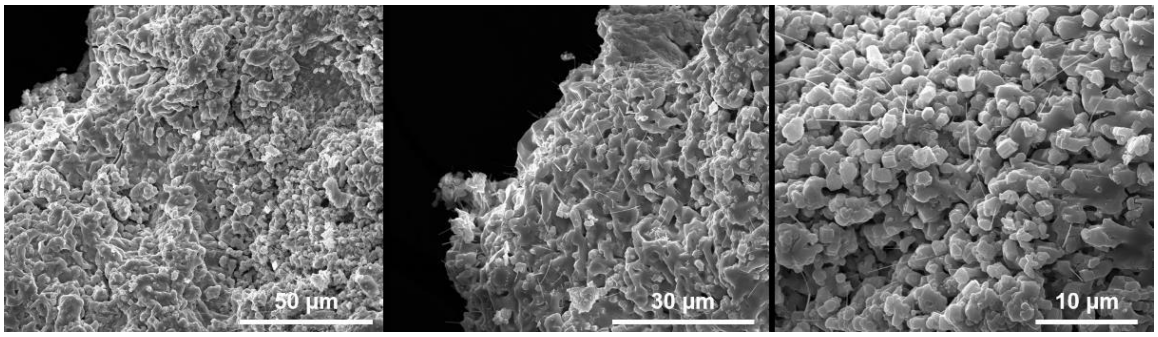

Figure 14. SEM images of the central channel surface of the SMO getter that was exposed to ~1 ppb $CrO_2(OH)_2$ (g) at 700 °C for 500 h: low (left), intermediate (medium), and high (right) magnification.

Thermal and hydrolytic stability of SMO getter: The structure of $SrMnO_3$ phase at high temperatures was investigated using in situ high-temperature (HT) XRD to observe any evidence of Sr segregation, such as the formation of SrO and $SrCO_3$, as well as phase separation, which often happens above 500 °C in Sr-containing perovskites. Figure 15 shows the in-situ HT–XRD patterns recorded at ~25, 500, 700, and 900 °C. The major five peaks at 2θ = 27, 33, 35, 43, and 49° in the initial XRD pattern (RT) were in good agreement with those of 4H perovskite $SrMnO_3$.

At elevated temperatures (500, 700, and 900 °C), no new peaks relating to SrCO3 and SrO phases were found despite collective peak shift caused by thermal expansion ($8.6 \cdot 10^{-6}$ K^{-1} by calculation), verifying the high thermal stability of $SrMnO_3$ without Sr-segregation. This result corresponds to the phase diagram of $SrMnO_3$, where the 4H–$SrMnO_3$ phase is regarded to be stable up to 1447 °C, and to the literature, which shows the stability of Sr-rich $Sr_xLa_{1-x}MnO_3$ (x = 0.4–0.8) up to 1000 °C. The stability of $SrMnO_3$ in humid atmosphere was also evaluated by comparing the structure of $SrMnO_3$ before and after its exposure to moisture which remains unchanged showing the resistant to water attack.

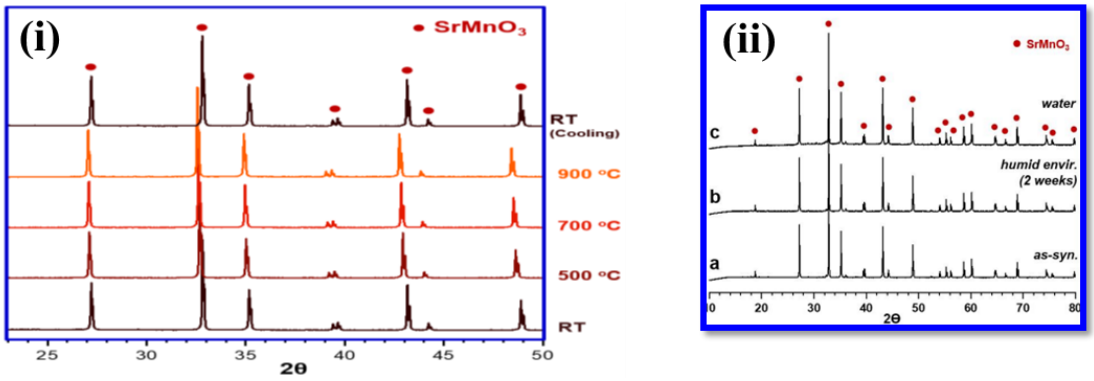

Figure 15. (i) High-temperature XRD patterns of $SrMnO_3$ powder: room temperature (RT), 500 °C, 700 °C, 900 °C, and RT after cooling down (ii) XRD patterns of (a) as-synthesized SrMnO3 powder, (b) the power placed in a humid environment for 2 weeks, and (c) the powder soaked in water for a day.

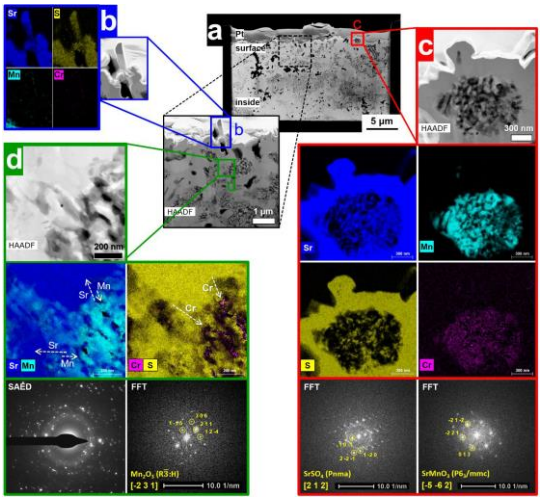

Figure 16. (a) High-angle annular dark-field (HAADF) STEM images of the cross-section of the sample taken from the inlet area of the SMO getter that was exposed to SO_2 gas and Cr vapor for 230 h at 700 °C during the EIS test. (b) Elemental mapping images (Sr, Mn, S, and Cr) of the nanorod grown on the surface by STEM-EDS. (c) Elemental mapping images of a particle protruding from the top surface of the getter and Fast-Fourier-Transform (FTT) patterns of high resolution (HR) TEM images of the particle. (d) Elemental mapping images and electron diffraction patterns (SAED and FFT) of the interface between the shell and the shell beneath the surface.

Figure 16 displays TEM and elemental mapping images of the cross-section of the inlet side of the getter section prepared by focused ion beam (FIB). Elemental images of the cross-section of a small particle protruding from the top surface of the getter reveals that the particle has a core-shell structure composed of a shell of Sr and S and a porous core of Mn and Cr. HR-TEM images of the surface area identify SO_2 (Pnma) and $SrMnO_3$ (P63/mmc) phases on the surface confirming the sulfur-capturing capability of the SMO getter. The elemental maps of porous area reveal that the absorbed Cr resides in the Mn-enriched porous core, whereas Sr and S are homogeneously distributed in the surrounding shell.

The structure of porous core was identified as nano-crystalline manganese oxides from halo rings and spots in the selected area electron diffraction (SAED) pattern, where Mn_2O_3 (space group R-3:H) is the most dominant phase among Mn oxides based on SAED and the phase diagram. It is considered that the Mn_2O_3 phase can accommodate Cr atoms as a form of $(Mn,Cr)_2O_3$ solid solution because of the very similar size of Cr and Mn ($^{VI}Cr^{3+}$ and $^{VI}Mn^{3+}$ radii are 0.615 Å and 0.580–0.645 Å, respectively), which is also supported by the phase diagram (Figure 17a). The above can be represented as per the reaction:

$$2SrMnO_3 + CrO_2(OH)_2\ (g) + SO_2\ (g) = SrCrO_4 + SO_2 + Mn_2O_3 + H_2O\ (g)$$

A phase stability diagram was developed as functions of the partial pressures of $CrO_2(OH)_2$ (g) and SO_2 (g) at 500–900 °C using the database in HSC chemistry 6 (Figure 17b). The major reaction associated with the phase transformation under the operating conditions are found as follows:

$$SrCrO_4 + SO_2\ (g) = SO_2 + ½Cr_2O_3 + ¼O_2\ (g)$$

Thermochemical data shows that, below 704 °C, $SrCrO_4$ is not very stable and is likely to react with SO_2 (g) (75 ppb) in ambient air, forming SO_2 in the end; simultaneously, segregated Cr can migrate to the Mn_2O_3 pocket.

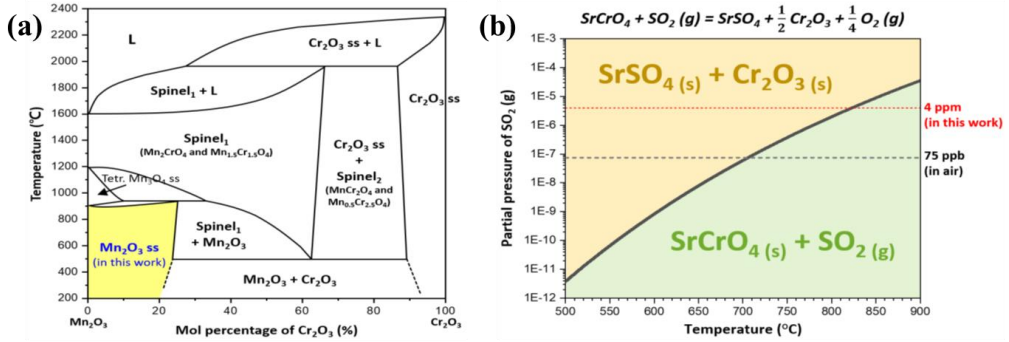

Figure 17. (a) Phase diagram for Mn_2O_3–Cr_2O_3 system (ss: solid solution; Tetr.: tetragonal; L: liquid). (b) Phase diagram as functions of the partial pressure of SO_2 (g) and temperature for the reaction between $SrCrO_4$ and SO_2 (g).

Furthermore, the Mn 2p core-level XPS spectra of $SrMnO_3$ (Figure 18a) shows better understanding of the absorption mechanism. The peak for Mn 2p3/2 (637–643 cm-1) shifts to lower binding energies with increasing depth, indicating the chemical state change of Mn ions from 4+ valance to +4/+3 mixed valance (i.e., from ideal $SrMnO_3$ to oxygen-deficient $SrMnO_{3-\delta}$). Additionally, the Raman spectrum (Figure 18b) of the $SrMnO_3$ pellet shows the signals for E1g

and A1g modes (434 and 634 cm^{-1}, respectively) of Mn_2O_9 moiety (= two of MnO_6 octahedra), confirming the existence of Mn_2O_9 dimers, as well as Sr, on the SMO surface.

The surface Mn_2O_9 tends to adsorb O_2 in air resulting in Mn-superoxo species which play an important role as a catalyst in oxidation and dehydrogenation. It is thus suggested that the Mn_2O_9 dimers on the surface have also functioned to facilitate the capturing of gaseous contaminants, especially for SO_2 as per the reaction:

$$Sr_{surface} + O_{2,adsorbed} + SO_2\ (g) \rightarrow SO_{2\ absorbed}$$

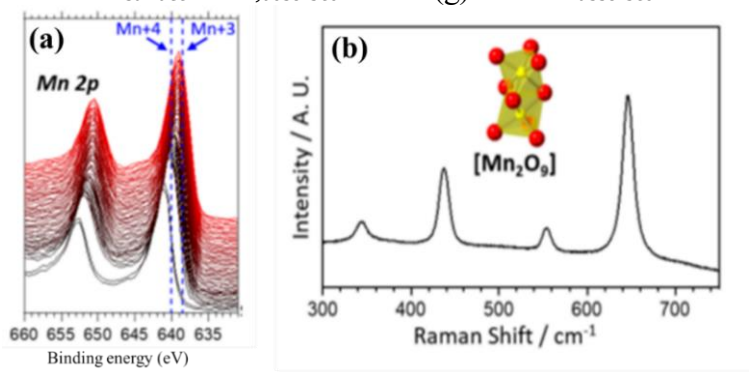

Figure 18. (a) Mn 2p core-level XPS spectra of $SrMnO_3$ pellet that was heat-treated at 700 °C for 100 h in ambient air and (b) Raman spectrum of the $SrMnO_3$ surface.

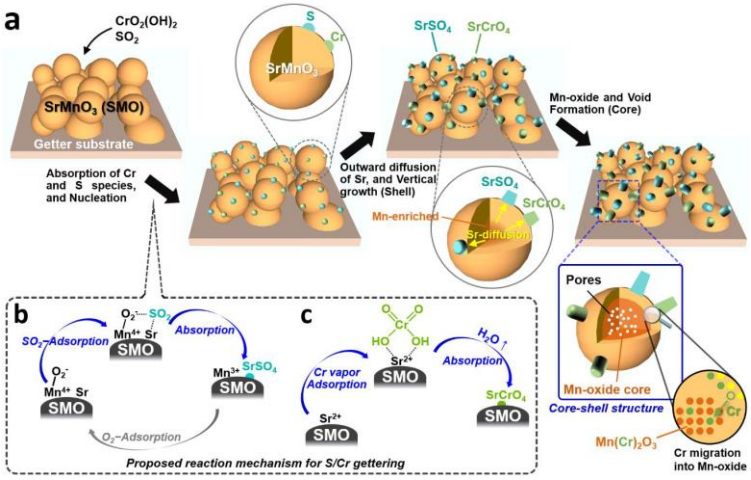

Figure 19. Schematic representation of the S/Cr capturing mechanism of SMO getter: (a) Capturing process accompanied by the vertical growth of reaction compounds and the formation of the core-shell structure, and the proposed reaction mechanisms for the absorption of (b) SO_2 and (c) $CrO_2(OH)_2$.

The trace contaminant capture on electrode surface is summarized in Figure 19. Under the flow of air stream containing gaseous S and Cr species, the Sr-terminated surface absorbs Cr vapor and SO_2 gas while the Mn_2O_9 dimers on the surface, along with Sr, assist the absorption reaction. The reaction of SMO with the absorbed S and Cr species results in the formation of $SrSO_4$ and $SrCrO_4$, respectively. The continued absorption occurs, accompanied by Sr diffusion toward the external surface, thus, leading to the vertical growth of SO_2 and $SrCrO_4$, and leaving voids and Mn-oxides at the core (where segregated Cr can reside).

The use of getter has demonstrated the successful capture of gaseous Cr and S contaminants under SOFC operating conditions. The application of the getter, fabricated from low-priced precursors via simple dip-coating process, provides a cost-effective solution to prevent the electrode poisoning without the need to replace the state-of-the-art component materials, thus making it suitable for large scale applications. For practical application, the modular design of the getter is considered useful since it can be replaced and disposed after its predetermined life. Modeling and simulation based on computational fluid dynamics (CFD) further help to design and optimize getter architectures depending on the scale and operating conditions of the system for a prolonged lifetime.

5.5 Task 5: Sensor development and integration in getter for *in-situ* monitoring

Impedance results on LSM/YSZ/LSM cells at 0.5 V bias shows a rapid decrease in the current when the electrode was exposed to the Cr vapor. In the absence of Cr vapor there is notable increase in the current which stabilizes over the time. It was further observed that upon exposing the electrodes to Cr vapor, leads to a sharp increase in the Rp (polarization resistance), mainly due to the charge and mass transport resistance because of chromium deposition. This distinct electrochemical behavior of the electrodes in the presence and absence of the Cr vapor was utilized as sensing device to sense Cr vapor along the getter length. Therefore, Cr and S sensitive materials such as LSM can be used in sensor cells. By the EIS measurement, the concentrations of sulfur and chromium vapor will be evaluated. Also, the lifetime of the getters can be calculated by the sensors.

5.5.1 Experimental methods & approaches:

A slurry paste of LSM was prepared using appropriate amount of Vehicle ink (FuelCells Energy) and was brush coated on one side of YSZ electrolyte (200 µm thickness). LSM electrode was sintered at 1200 °C with the heating rate of 3 °C/min. Pt ink was also brush coated on the YSZ electrolyte as reference electrode (RE) as shown in the Figure 20 (a). Sensor with Pt leads were attached and sintered at 850 °C for 1h to get the final sensor configuration (Figure 20 (b)). The fabricated device was validated using the experimental setup as shown in the Figure 20(c) in the presence of 3% H_2O air with/without Cr. The sensor device was tested at 850 °C and the air flow rate was maintained at 50 sccm. Initially, the device was tested at different bias for validation.

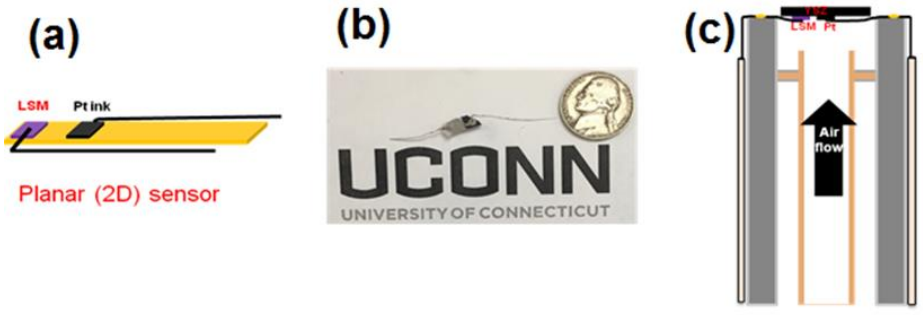

Figure 20. (A) Schematic of the planar sensor configuration with LSM as sensing electrode (SE) and Pt as reference electrode (RE), (B) Digital image of the sensor device, (C) Schematic illustration of the sensor validation test experiment.

The morphological and elemental analyses were performed using an FEI Quanta 250 FEG scanning electron microscope (SEM) attached with an energy dispersive X-ray spectroscope (EDS). Electrochemical performance of sensor device was measured using a multi-channel potentiostat (VMP2, Bio-Logic). The current was recorded every minute. A bias of 250 mV was applied between the cathode and the reference. The electrochemical impedance spectra (EIS) were measured in the frequency range from 100 mHz to 200 kHz with a 10 mV sinus amplitude at an interval of 1 h.

5.5.2 Results & discussion

Figure 21 shows I-t curves of sensor tests performed in 3% H_2O air under a cathode flow rate of 50 sccm with 100 mV bias and 850°C ran for short duration of 24 h. The experiment validates the operation of the planar sensor configuration. The I-t data shows a stable performance during the 24 h test study. Further, the tests were also conducted with different bias applied such as 0, 250 and 500 mV and they show stable performance during 24 h study.

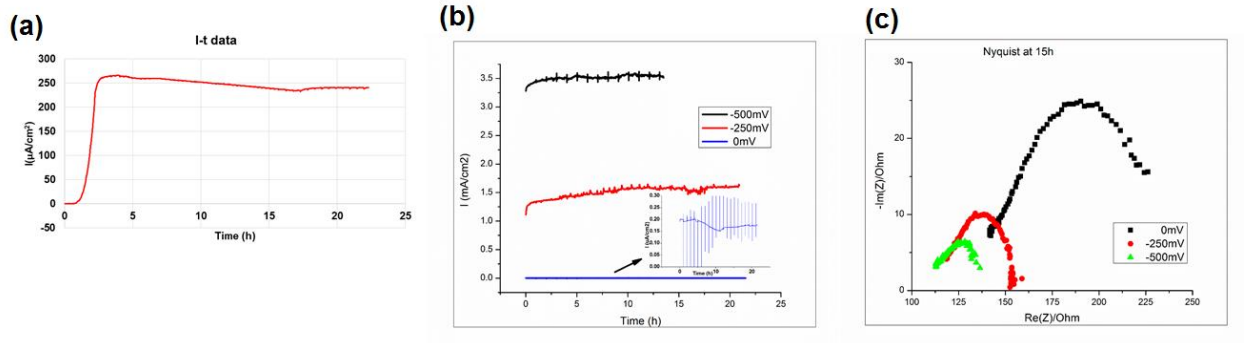

Figure 21. Current vs. Time (I-t) plot of the sensor device with stable performance for 24 h. (a) I-t data at 100mV bias, (b) I-t data at 0, 250 and 500 mV bias applied and (c) Nyquist spectra for different bias.

6 Summary and conclusions

The research program developed and validated the efficacy of getter technology for the co-capture of intrinsic and extrinsic ambient air stream contaminants to mitigate the electrochemical performance degradation in high temperature solid oxide fuel cell systems. Experimental findings of the study show that the gas phase acidic airborne impurities react with the basic air electrode constituents to form stable reaction products at the free surface (gas-solid interface) and electroactive triple phase boundary (electrode-electrolyte-gas) resulting in rapid degradation of the electrochemical performance. High surface getter material using Gr II alkaline earth and transition metal oxides offering oxide basicity and ability to capture acidic impurities before interacting with air-electrode were developed. Thermodynamic calculations based on Gibbs free energy minimization validated the co-capture of sulfur and chromium impurities in wide temperature range based on minimization of free energy of solid-gas reactions and formation of reaction products. Cost-effective high surface area SMO based getter synthesis procedure has been developed in the laboratory and demonstrated for large scale production. The efficacy of the getter has been validated electrochemically under SOFC operating conditions. Posttest characterization results indicate clean LSM/YSZ interface after 100 hrs of electrochemical test in the presence of

Cr and SO_2 vapor while analysis of the SMO getter reveals high concentration of S and Cr at the inlet of the getter only. SMO also showed excellent thermal and hydrolytic stability with no phase transformation and hydrolysis during exposure to high-temperatures and humid environments, fulfilling the requirement for the operation in high-temperature electrochemical systems.

Products

a. Publications, conference papers, and presentations

i) Journal publications:

1. J. Hong, A.N. Aphale S.J. Heo, B. Hu, M. Reisert, S. Belko, and P. Singh, "Strontium Manganese Oxide Getter for Capturing Airborne Cr and S Contaminants in High-Temperature Electrochemical Systems" ACS applied materials & interfaces, 11(38), (2019) 34878-34888.
2. S.J. Heo, J. Hong, A. Aphale, B. Hu, and P. Singh, "Chromium Poisoning of La1-xSrxMnO3±δ Cathodes and Electrochemical Validation of Chromium Getters in Intermediate Temperature-Solid Oxide Fuel Cells" Journal of The Electrochemical Society, 166(13), (2019)
3. Hong, Junsung, Su Jeong Heo, and Prabhakar Singh. "Combined Cr and S Poisoning Behaviors of $La_{1-x}Sr_xMnO_{3\pm\delta}$ and $La_{1-x}Sr_xCo_{1-y}Fe_yO_{3-\delta}$ Cathodes in Solid Oxide Fuel Cells." *Applied Surface Science* (2020): 147253.
4. Hong, J, Anisur, M. R., Heo, S J, Dubey, P K, and Singh, P. Sulfur Poisoning and Performance Recovery of SOFC Air Electrodes. Frontiers in Energy Research, 9, 2021.

ii) Books or other non-periodical, one-time publications:

iii) Other publications, conference papers and presentations:

1) Conference paper

1. Junsung Hong, Su Jeong Heo, Ashish N. Aphale, Boxun Hu, Prabhakar Singh, Cathode Poisoning and Mitigation in the Presence of Combined Cr and S Contaminants in SOFC , Presenting at the 2019 TMS Annual Meeting & Exhibition, TX, USA.
2. M. A. Uddin, C. Banas, C. Liang, U. Pasaogullari, K. Recknagle, B. Koeppel, J. Stevenson, and P. Singh, Design and Optimization of Chromium Getter for SOFC Systems through Computational Modeling, Presented at the 15th International Symposium on Solid Oxide Fuel Cells (SOFC-XV), July 23-28, 2017, Hollywood, FL.
3. Md Aman Uddin, Ashish Aphale, Boxun Hu, Ugur Pasaogullari and Prabhakar Singh, In-cell Chromium Getters to Mitigate Cathode Poisoning in SOFC Stack, Presented at the 15th International Symposium on Solid Oxide Fuel Cells (SOFC-XV), July 23-28, 2017, Hollywood, FL.
4. Boxun Hu, Su Jeong Heo, Junkai He, Yanliu Dang, Ashish Aphale, Aman Uddin, Junsung Hong, Justin Webster, Seraphim Belko, Steven L. Suib, and Prabhakar Singh, High Surface Area Getter Materials for Chromium and Sulfur Capture in SOFC Systems, Presented at the 18th Annual Solid Oxide Fuel Cell (SOFC) Project Review Meeting, Pittsburgh June 12-14, 2017.
5. Su Jeong Heo, Boxun Hu, Ashish Aphale, Aman Uddin and Prabhakar Singh, Low-Temperature Chromium Poisoning of SOFC Cathode, 15th International Symposium on Solid Oxide Fuel Cells (SOFC-XV), July 23-28, 2017, Hollywood, FL.

b. Website(s) or other Internet site(s): None

c. Technologies or techniques: None

d. Inventions, patent applications, and/or licenses: None

e. Other products: None

Training and Professional Development

One post-doctoral fellow has been trained to perform the modelling work. The graduate students are being trained with experimental methods and analytical tools. The post-doctoral fellow and the students are being educated with the fuel cell knowledge.

Participants and Other Collaborating Organization

Prof. Prabhakar Singh
Project role: Principal investigator
Contribution to project: Provide guidance and oversee the project

Prof. Steven L. Suib
Project role: Co-investigator
Contribution to project: Leading the high surface area materials synthesis.

Dr. Boxun Hu
Project role: Co-investigator
Contribution to Project: Leading experimental research through planning, training graduate students, analyzing the results, and interfacing with the team.

Dr. Ashish Aphale
Project role: Post-doctoral fellow
Contribution to Project: Conducting the experiments, analyzing the data.

Dr. Md. Uddin
Project role: Post-doctoral fellow
Contribution to Project: Conducting computation modelling.

Mr. Junkai He
Project role: Graduate student
Contribution to Project: Conducting getter material synthesis and characterization.

Ms. Yanliu Dang
Project role: Graduate student
Contribution to Project: Conducting getter material synthesis and characterization.

Impact

The impact of the project findings is multifaceted.

- Potential benefits and outcomes of this project will mitigate the LSM and LSCF degradation arising due to the presence of moisture, sulfur, and chromium species in the 'real world' cathode environment.
- Mitigation of the cathode degradation will significantly increase the performance stability and long-term reliability of SOFC thus accelerating the demonstration and commercial deployment of the technology to the technology readiness level (TRL) from 2 to 5.
- The research effort focused on developing methodology for the selection and optimization of high surface area getter materials for mitigation of surface segregation and compound formation.
- Cost effective Cr-S getter materials and architectures developed for application in stacks and BOP.
- Graduate students and post-doctoral fellows were trained under this project.

Changes/Problems

There is no change on the goals of the project as well as experimental plans so far.

Special Reporting Requirements

Not Applicable

References

[1] R C Ropp. Encyclopedia of the Alkaline Earth Compounds. Elsevier; 2013. https://doi.org/10.1016/C2012-0-00777-6.

[2] Gasik MI. Technology of Chromium and Its Ferroalloys. Handb. Ferroalloys, Elsevier; 2013, p. 267–316. https://doi.org/10.1016/B978-0-08-097753-9.00008-3.

[3] Negas T, Roth RS. The system SrO-"chromium oxide" in air and oxygen. J Res Natl Bur Stand Sect A Phys Chem 1969;73A:431. https://doi.org/10.6028/jres.073A.034.

[4] Hong J, Aphale AN, Heo SJ, Hu B, Reisert M, Belko S, et al. Strontium Manganese Oxide Getter for Capturing Airborne Cr and S Contaminants in High-Temperature Electrochemical Systems. ACS Appl Mater Interfaces 2019;11:34878–88. https://doi.org/10.1021/ACSAMI.9B09677.

[5] Aphale A, Hong J, Hu B, Singh P. Development and Validation of Chromium Getters for Solid Oxide Fuel Cell Power Systems. J Vis Exp 2019. https://doi.org/10.3791/59623.

[6] Wang CC, Chen K, Jiang SP. Mechanism and Kinetics of SO2 Poisoning on the Electrochemical Activity of La0.8Sr0.2MnO3 Cathodes of Solid Oxide Fuel Cells. J Electrochem Soc 2016;163:F771. https://doi.org/10.1149/2.0221608JES.

[7] Daio T, Mitra P, Lyth SM, Sasaki K. Atomic-resolution analysis of degradation phenomena in SOFCS: A case study of SO2 poisoning in LSM cathodes. Int J Hydrogen Energy 2016;41:12214–21. https://doi.org/10.1016/J.IJHYDENE.2016.05.216.

[8] Zhao L, Zhang J, Becker T, Jiang SP. Raman Spectroscopy Study of Chromium Deposition on La0.6Sr0.4Co0.2Fe0.8O3-δ Cathode of Solid Oxide Fuel Cells. J Electrochem Soc 2014;161:F687. https://doi.org/10.1149/2.018406JES.

[9] Chen X, Jin C, Zhao L, Zhang L, Guan C, Wang L, et al. Study on the Cr deposition and poisoning phenomenon at (La0.6Sr0.4)(Co0.2Fe0.8)O3−δ electrode of solid oxide fuel cells by transmission X-ray microscopy. Int J Hydrogen Energy 2014;39:15728–34. https://doi.org/10.1016/J.IJHYDENE.2014.07.112.

[10] Hu B, Krishnan S, Liang C, Heo SJ, Aphale AN, Ramprasad R, et al. Experimental and thermodynamic evaluation of La1−xSrxMnO3±δ and La1−xSrxCo1−yFeyO3−δ cathodes in Cr-containing humidified air. Int J Hydrogen Energy 2017;42:10208–16. https://doi.org/10.1016/J.IJHYDENE.2017.01.040.

[11] Wang F, Yamaji K, Cho D-H, Shimonosono T, Nishi M, Kishimoto H, et al. Evaluation of Sulfur Dioxide Poisoning for LSCF Cathodes. Fuel Cells 2013;13:520–5. https://doi.org/10.1002/FUCE.201200172.

[12] Wang F, Yamaji K, Cho DH, Shimonosono T, Kishimoto H, Brito ME, et al. Effect of strontium concentration on sulfur poisoning of LSCF cathodes. Solid State Ionics 2012;225:157–60. https://doi.org/10.1016/J.SSI.2012.05.026.

[13] Yang Z, Guo M, Wang N, Ma C, Wang J, Han M. A short review of cathode poisoning and corrosion in solid oxide fuel cell. Int J Hydrogen Energy 2017;42:24948–59. https://doi.org/10.1016/J.IJHYDENE.2017.08.057.

[14] Jiang SP, Zhang S, Zhen YD. Deposition of Cr Species at (La, Sr)(Co, Fe)O3 Cathodes of Solid Oxide Fuel Cells. J Electrochem Soc 2005;153:A127. https://doi.org/10.1149/1.2136077.

[15] Zhang HH, Zeng CL. Preparation and performances of Co–Mn spinel coating on a ferritic stainless steel interconnect material for solid oxide fuel cell application. J Power Sources 2014;252:122–9. https://doi.org/10.1016/J.JPOWSOUR.2013.12.007.